

Article

Thermal Hysteresis Control in Fe₄₉Rh₅₁ Alloy through Annealing Process

Vladimir Rodionov¹, Abdulkarim Amirov^{1,2,*} , Murad Annaorazov¹, Erkki Lähderanta³ , Alexander Granovsky⁴, Akhmed Aliev^{1,2} and Valeria Rodionova¹ 

¹ Institute of Physics, Mathematics and Informational Technology, Immanuel Kant Baltic Federal University, 236016 Kaliningrad, Russia; VLRodionov@kantiana.ru (V.R.); annaoraz@hotmail.com (M.A.); lowtemp@mail.ru (A.A.); vvrodionova@kantiana.ru (V.R.)

² Amirkhanov Institute of Physics of Dagestan Federal Research Center, Russian Academy of Sciences, Yaragskogo 94, 367003 Makhachkala, Russia

³ Department of Physics, LUT-University, 53851 Lappeenranta, Finland; Erkki.Lahderanta@lut.fi

⁴ Faculty of Physics, Lomonosov Moscow State University, Leninskie Gory 1-2, 119991 Moscow, Russia; granov@magn.ru

* Correspondence: amiroff_a@mail.ru

Abstract: We report the results of studies of the magnetic and transport properties of Fe₄₉Rh₅₁ alloy prepared by different sequences of quenching and the annealing process. The temperature dependences of the relative initial magnetic permeability and resistivity are analyzed. An optimal regime consisting of annealing at 1300 K for 440 min and quenching from 1300 K to 275 K is found to observe the desired narrow antiferromagnetic–ferromagnetic transition in Fe₄₉Rh₅₁ alloy under cyclic conditions. This has the potential to increase the efficiency of cooling devices based on the magnetocaloric effect of magnetic materials with a first-order field-induced phase transition.

Keywords: Fe–Rh; first-order magnetic phase transition; heat treatment; thermal hysteresis



Citation: Rodionov, V.; Amirov, A.; Annaorazov, M.; Lähderanta, E.; Granovsky, A.; Aliev, A.; Rodionova, V. Thermal Hysteresis Control in Fe₄₉Rh₅₁ Alloy through Annealing Process. *Processes* **2021**, *9*, 772. <https://doi.org/10.3390/pr9050772>

Academic Editor: Andrea Petrella

Received: 1 October 2020

Accepted: 20 April 2021

Published: 28 April 2021

Publisher's Note: MDPI stays neutral with regard to jurisdictional claims in published maps and institutional affiliations.



Copyright: © 2021 by the authors. Licensee MDPI, Basel, Switzerland. This article is an open access article distributed under the terms and conditions of the Creative Commons Attribution (CC BY) license (<https://creativecommons.org/licenses/by/4.0/>).

1. Introduction

Since the discovery of the giant magnetocaloric effect (MCE) in near-equiatomic Fe–Rh alloys there has been increasing interest in the study of these compounds [1,2]. Up to now, Fe–Rh has had the record value for adiabatic temperature change at reasonable magnetic fields [3–5]. Moreover, Fe–Rh alloys also exhibit anomalies of magnetic [4,6], thermal [7–9], and transport [6,9,10] properties around the temperature of magnetostructural transition. Despite the giant values of the magnetocaloric and elastocaloric effects in these alloys, they cannot be regarded as promising prospects for use in magnetic cooling due to the reduction of the magnetocaloric effect in cyclic magnetic fields as well as due to the existence of thermal hysteresis [5,9]. Future challenges in studies of Fe–Rh alloys may involve searching for methods to increase their stability in cyclic magnetic fields in order to decrease the thermal hysteresis of transition. Among the different methods employed to control magnetic properties, and one of the simplest and most commonly used, is heat treatment [11].

Near-equiatomic Fe–Rh alloy is characterized by CsCl-type crystal structures (α or B2) with a first-order metamagnetic phase transition around $T_m \sim 360$ K (upon heating) from the antiferromagnetic (AFM) phase to the ferromagnetic (FM) one. The transition is accompanied by a sharp increase in the magnetization [12,13], lattice parameter [14–16], specific heat [4,9,11,17], and entropy [18,19]. Furthermore, there is no change in the crystal symmetry of Fe–Rh alloys during the AFM–FM transition, while the volume expansion on transition is about 1% [20]. There are numerous methods to control the magnetic phase transition parameters and the MCE in Fe–Rh, including the use of magnetic fields [21], hydrostatic pressure [22,23], electric field-induced strain [24–26], mechanical and heat treatments [4,13,21,27–29], chemical substitution [30,31], and ion irradiation [13,32]. While

the effects of external influences (such as magnetic fields and pressure) on the transition temperature is relatively clear, there is less information about how the process of heat treatment affect the phase transition in Fe–Rh alloys. Based on treatment conditions, authors reported either the independence of the transition temperature of Fe₄₉Rh₅₁ alloy [21], or a shift of the transition temperature to higher [14,20] or lower [22,28,33] temperatures. That is why establishing appropriate annealing and quenching protocols can help to shift the transition or to stabilize it. Moreover, using thermal treatment protocols, possible disadvantages for applications (e.g., a wide range of transition and thermal hysteresis, irreversibility, or degradation under cycling in the magnetic field [5,9,34]) can be overcome. A phase transition having a near-zero width of thermal hysteresis and occurring in a narrow temperature range can be referred to as the “model”. In materials with the parameters of the first-order magnetic phase transition closer to the “model”, the large magnetocaloric effect is expected [4,6].

This work is aimed to define the optimal protocol for the thermal treatment of Fe–Rh alloys to reach a decrease in both thermal hysteresis width and transition temperature range.

2. Materials and Methods

The Fe₄₉Rh₅₁ alloys were synthesized by induction melting of high-purity Rh (99.90%) and Fe (99.98 %) metals in an argon atmosphere at a pressure of 100 kPa using a furnace with arc and induction melting options (Oxford, ME, USA) The ingot was cleaned using conventional chemical and mechanical treatments and annealed at 1273 K for 45 h in vacuum. Subsequently, the ingot was cut into rectangular samples with dimensions 14 × 4 × 0.27 mm³. The chemical composition of the samples was examined using a scanning electron microscope (JSM-6390LV) integrated with an energy dispersive X-ray spectroscopy (EDX) analyzer (Oxford X-Acta, Abingdon, UK) and determined to be Fe₄₉Rh₅₁. The details of fabrication were described earlier [4]. In the present study, we focus on the improvement of a thermal treatment protocol and study its influence on thermal hysteresis parameters.

Magnetic measurements were carried out using the induction method [35]. Resistivity was measured using the standard four-contact potentiometric method at a current of 0.1 A in the temperature range of 290–1400 K. Before each measurement, the samples were cooled to a temperature far lower than the phase transition temperature to reach the AFM state. The rate of temperature change was ~2 K/min.

The following thermal treatment protocol was used. First, samples were annealed at 1273 K for 72 h, followed by a slow cooling to room temperature. Quenching was done through the following steps: heating up to T_1 , exposing samples to this temperature for t minutes, slow cooling down to T_2 , quenching in the medium with T_3 , and slow cooling (or heating) to room temperature. The average cooling (or heating) rate was ~100 K/h. Quenching was carried out in water, oil, Ga, and air. The influence of the quenching protocol on the AFM–FM transition parameters was studied by analyzing the temperature dependences of the initial magnetic permeability $\mu(T)$ and, in some cases, resistivity $\rho(T)$ curves.

3. Results and Discussion

Figure 1 shows the temperature dependence of resistivity for a sample in cooling and heating protocols. The resistivity ρ decreased abruptly in the temperature range of 327–375 K (read line, heating), indicating the transition from AFM to FM state. The temperature $T_M^{heat} = 353$ K corresponded to the minimum $\rho(T)$ in this range. Further heating resulted in an increase of the resistivity $\rho(T)$ with a maximum at around of $T_C = 642$ K. This corresponded to the transition into the paramagnetic (PM) state. Further heating up to ~1300 K led to slow decreases in resistivity.

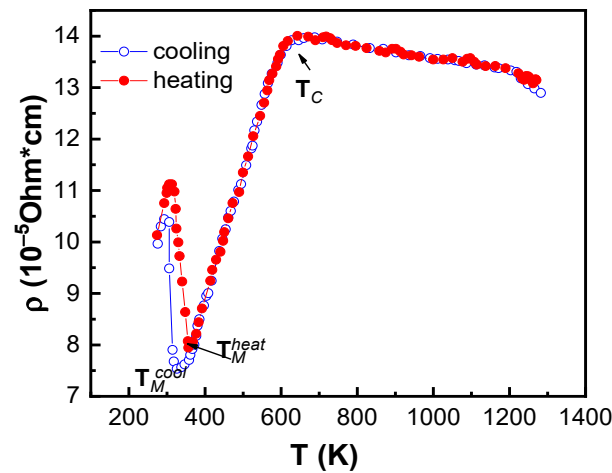


Figure 1. Temperature dependence of resistivity for an annealed (at 1273 K for 72 h) and slowly cooled sample.

Under cooling of the sample from high temperatures, the nonhysteretic second-order phase transition from PM to FM state occurred at $T_C \sim 642$ K and the first-order phase transition from FM to AFM state took place in the temperature range of 330–308 K with the transition temperature $T_M^{cool} = 319$ K.

Thus, the studied alloy in the 290–1300 K temperature range could be in three different magnetic states, AFM, FM, and PM in the ordered bcc α (B2) structural state, according to the phase diagram [36,37]. However, in this temperature range, where the $\text{Fe}_{49}\text{Rh}_{51}$ should only be in a bcc B2 phase, the coexistence of the paramagnetic face-centered cubic (fcc) impurity γ (A1) phase was observed [28,29].

It is evident that in this temperature range the alloy undergoes the isomorphous AFM–FM and FM–PM transitions and, apparently, some structural state changes with phase decomposition [28,29]. The intergranular interactions between the paramagnetic γ phase and the ordered magnetic α phase were considered by Chirkova [28], and locally induced stresses on grains during the α phase were pointed as a stimulus for the tuning of the magnetic properties of the Fe–Rh alloy. Annealing at different temperatures led to the redistribution of the γ phase and resulted in the changing of internal stresses. Therefore, to clarify the influence of quenching on the AFM–FM transition parameters (e.g., transition temperatures, width of hysteresis, and transition region), the quenching processes were subsequently carried out employing several temperatures in the high-temperature (HT) region as well as at lower temperatures, using temperature changes corresponding to the following transitions: FM \rightarrow AFM, PM \rightarrow AFM, PM \rightarrow FM, HT \rightarrow AFM, HT \rightarrow FM, HT \rightarrow PM, where HT is a high-temperature region of 1200–1400 K. The HT region was selected as region where the stable B2 phase is expected [28].

As seen from Figure 2, the quenching from the FM and PM states to the AFM state shifted the thermal hysteresis loop toward low temperatures by 5–6 K without a change in the hysteresis width $\tau = 24$ –25 K. Similar results were obtained for quenching from temperatures close to the HT region. Quenching from within the HT region led to an extremely sharp AFM–FM transition (Figure 3). The sharpness of the transition observed in the $\mu(T)$ and $\rho(T)$ curves was increased with an increase in the upper quenching temperature (Figure 4) and was almost independent of lower quenching temperatures. However, the location of the transition area depends on the lower temperature of quenching. The dependence of the transition parameters from upper quenching temperatures was also observed on $\rho(T)$ curves by Takahashi et al. [29] for samples quenched at 970 K and 1070 K.

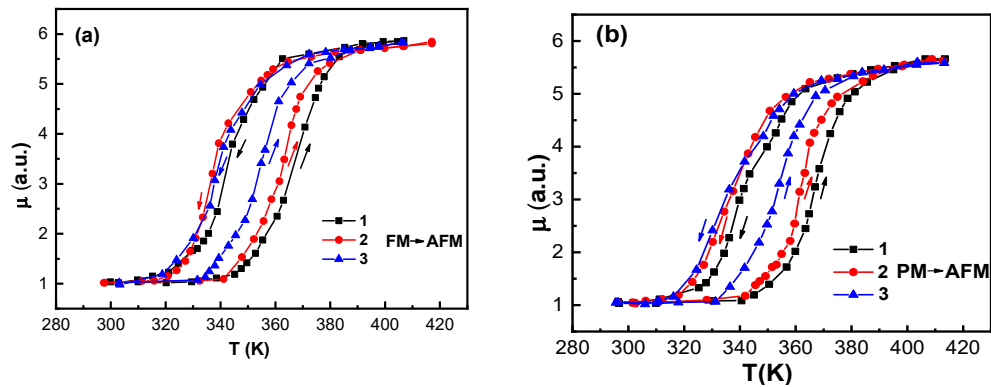


Figure 2. Temperature dependences of the relative initial magnetic permeability for two samples of $\text{Fe}_{49}\text{Rh}_{51}$ alloy: 1. after annealing at 1273 K for 72 h and being slowly cooled; 2. after quenching (a) from 473 K down to 278 K and (b) from 723 K down to 278 K; 3. after two cycles of heating and cooling in the 273–513 K temperature interval.

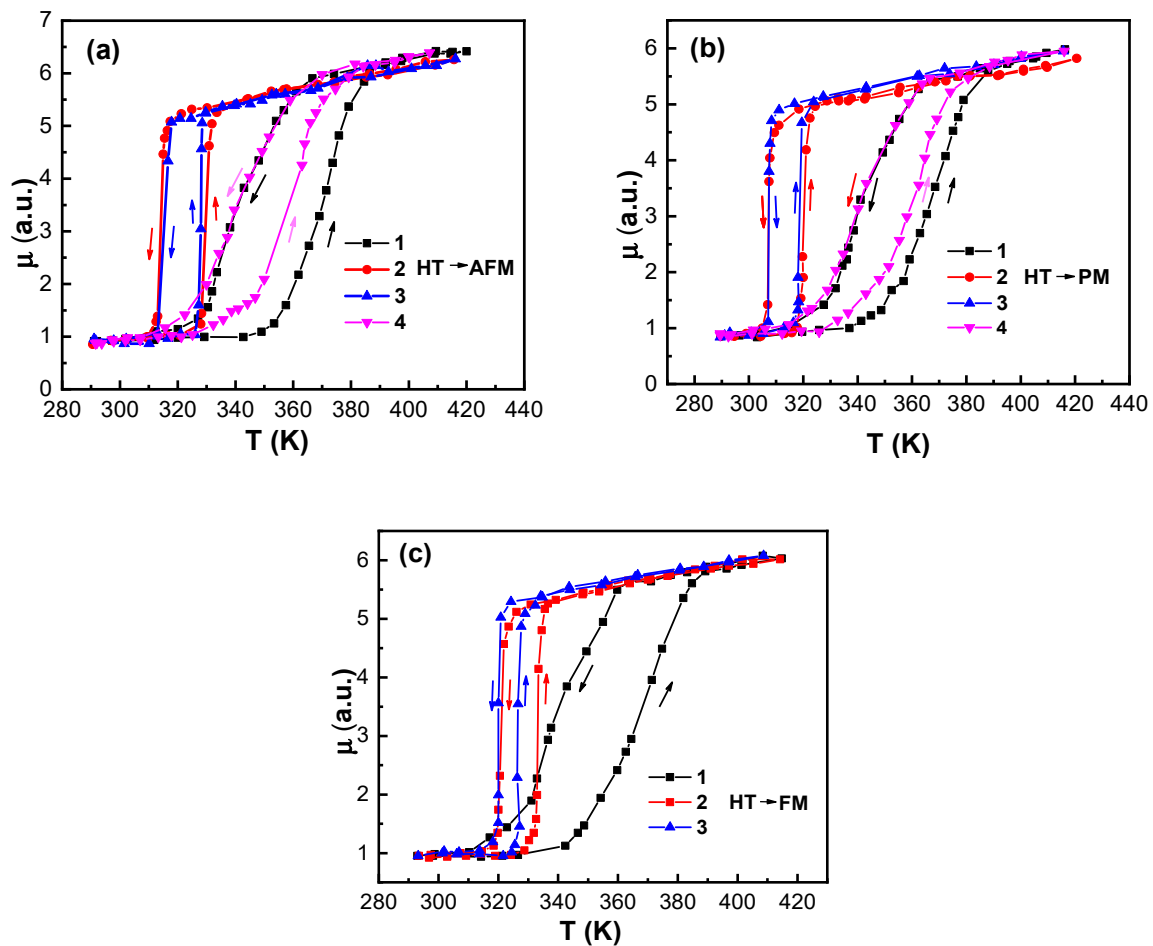


Figure 3. Temperature dependences of the relative initial magnetic permeability for samples of $\text{Fe}_{49}\text{Rh}_{51}$ alloy: 1. after annealing at 1273 K for 72 h and being slowly cooled; 2. after quenching (a) from 1273 K down to 278 K, (b) from 1273 K down to 773 K, and (c) from 1273 K down to 473 K; 3. and 4. after 2 cycles of heating and cooling in the 273–513 K temperature interval.

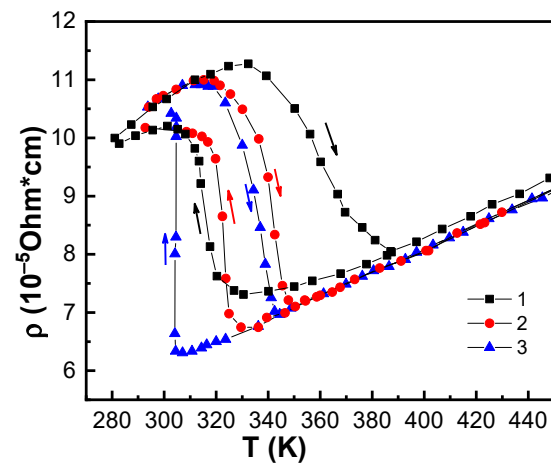


Figure 4. Temperature dependences of resistivity for samples of $\text{Fe}_{49}\text{Rh}_{51}$ alloy: 1. annealed at 1273 K for 72 h and slowly cooled; 2. quenching from 1073 K down to 290 K; 3. quenching from 1371 K down to 990 K.

Figure 5 depicts the temperature dependences of the magnetic permeability μ for samples of $\text{Fe}_{49}\text{Rh}_{51}$ alloy with different exposure times. A typical quenching curve was obtained for a short exposure time of 5 min at T_1 . In this instance, the hysteresis area was slightly different from that of annealed and slowly cooled samples. The shift of the hysteresis area of quenched samples toward lower temperatures was observed for an exposure time of at least 440 min. Moreover, the tendency of the μ jump to decrease for quenched samples was observed with an increase in exposure time, and, therefore, with a decrease in the transition temperature.

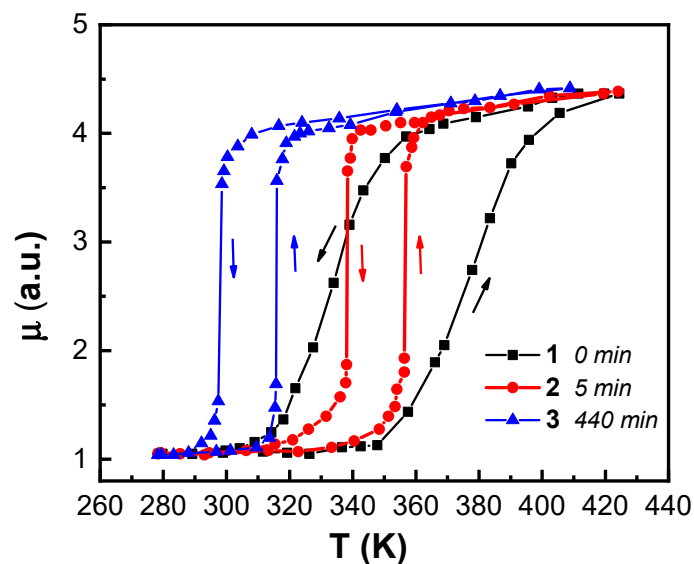


Figure 5. Temperature dependences of the relative initial magnetic permeability for samples of $\text{Fe}_{49}\text{Rh}_{51}$ alloy: 1. after annealing at 1273 K for 72 h and being slowly cooled; 2. after quenching from 1300 K down to 275 K with an exposure time of 5 min at 1300 K; 3. after quenching from 1300 K down to 275 K with an exposure time of 440 min at 1300 K.

The results of the quenching experiments are summarized in Table 1. As can be seen, the best results with regards to transition parameters (transition range and hysteresis width) were demonstrated in samples 6 and 7, which were quenched in water (275 K) from an upper temperature of 1300 K. It should be noted that sample 5 also showed a narrow hysteresis width of about 6.3 K, but the transitions in samples 6 and 7 were more acute.

Both samples 6 and 7 had similar hysteresis widths of 6.9 K and 7 K, respectively; however, the shape of transition for sample 7 was closer to the “model”. We compared the observed results for sample 7 with the literature data, where similar heat treatment protocols were used. Similar results were observed for Fe_{49.5}Rh_{50.5} samples annealed at 1370 K for 48 h in a vacuum and quenched in water, resulting in a sharp transition in the 300–309 K range and a narrow hysteresis width of about 9 K [29]. In addition, results on quenched samples of Fe₄₉Rh₅₁ have been reported with a hysteresis width of about 6 K, which is bit better than for our samples 6 and 7 [17]. However, the transition range for our samples was narrower.

Table 1. The influence of the heat treatment on the parameters of the AFM–FM transition in Fe₄₉Rh₅₁ alloy: T₁, annealing temperature, t, exposure time, T₂ and T₃, upper and lower quenching temperatures, T_{AFM–FM} (T_{FM–AFM}), AFM–FM (FM–AFM) transition temperature before heat treatment, T'_{AFM–FM} (T'_{FM–AFM}). AFM–FM (FM–AFM) transition temperature after heat treatment; τ and τ', hysteresis width before and after heat-treatment.

№	T ₁ , K	t, min	T ₂ , K	T ₃ , K	Treatment Protocol	T _{AFM–FM} , K	T' _{AFM–FM} , K	T _{FM–AFM} , K	T' _{FM–AFM} , K	τ, K	τ', K
						Before	After	Before	After	Before	After
1	-	-	-	-	Annealing 1273 K, 72 h, cooling to RT with rate ~100 K/h	371.8	358.5	344.8	345.4	27.0	13.1
	1273	35	1273	473	Quenching in oil	334.2	332.3	321.2	321.7	13.0	10.6
2	-	-	-	-	Annealing 1273 K, 72 h, cooling to RT with rate ~100 K/h	369.4	359.8	344.4	345.2	25.0	11.6
	1273	35	1273	274	Quenching in water	325.2	324.2	313.2	313.2	12.0	11.0
3	-	-	-	-	Annealing 1273 K, 72 h, cooling to RT with rate ~100 K/h	368.6	-	343.2	-	25.4	-
	1273	35	513	275	Quenching in water	362.2	354.2	337.2	338.4	25.0	15.8
4	-	-	-	-	Annealing 1273 K, 72 h, cooling to RT with rate ~100 K/h	367.8	-	344.2	-	23.6	-
	1273	35	723	278	Quenching in water	362.8	355.6	341.0	339.1	21.8	16.5
5	-	-	-	-	Annealing 1273 K, 72 h, cooling to RT with rate ~100 K/h	368.2	-	341.9	-	26.3	-
	1273	60	1258	753	Quenching in liquid Ga	337.5	331.6	325.4	329.3	12.1	6.3
6	1300	5	1300	275	Quenching in water	339.5	333.7	325.8	326.8	13.7	6.9
7	1300	440	1300	275	Quenching in water	324.7	318.0	311.0	311.0	13.7	7.0
8	-	-	-	-	Annealing 1273 K, 72 h, cooling to RT with rate ~100 K/h	353.2	-	319.1	-	34.1	-
9	1371	-	1208	789	Quenching in air	333.0	-	317.0	-	16.0	-
	1371	-	1364	987	Quenching in air	323.2	320.7	303.2	303.4	20.0	17.3

The influence of quenching on the AFM–FM transition parameters in Fe–Rh alloys has been previously discussed [14,16,20–22,33,34]. In [38], the decreasing of the transition temperature was explained by the quenching of small regions of the sample, which kept the ferromagnetic state down to low temperatures. These regions hinder the transition of the AFM matrix to the FM state when heating. But our results demonstrate that annealing in a certainly paramagnetic region (~990 K), followed by slowly passing through the ferromagnetic region, results in a typical quenching curve (Figure 4, curve 3), while the quenching from 1073 K to water (290 K) does not result in this type of curve (Figure 4, curve 2). The Curie temperature T_C of the alloy estimated from Figure 1 is 642 K. Consequently, a strong sharpening of the transition and shift of the transition area toward low temperatures cannot be explained by the formation and stabilization of small ferromagnetic nucleuses during the quenching process. In [16] the results of quenching experiments were explained by remnant deformations that appeared under sharp cooling of samples. Similar results were obtained in [34,39], where the influence of the nonmagnetic impurity phase on FM–AFM transition was experimentally and theoretically studied in Fe–Rh alloys.

In total, the analysis of reported literature data does not allow us to conclude which protocols demonstrate the best critical parameters (hysteresis width and transition range). These parameters, as well as other magnetic characteristics, strongly depend on the fabrication method, conditions of heat treatment protocol (temperature, time, and cooling rate), and thermomagnetic history of samples. Reported parameters obtained differ in measurements (resistivity, magnetization, and calorimetry), which complicates comparisons. Magnetic fields shift the transition temperatures and affect the hysteresis width, as exemplified in [17] where it was demonstrated that a 1 T magnetic field suppresses hysteresis up to 6 K compared to 6.5 K when using the same measurements with a 0.1 T field. In addition, there is not a uniform model to explain the influence of heat treatment conditions on transition parameters. Most reported results show that the quenched samples have an optimal for practical applications parameters of magnetic phase transition. In the high-temperature region, a slow transition to a single-phase (structurally homogeneous) state occurs throughout the entire volume of the sample. Rapid quenching makes it possible to preserve the homogeneous structure of the alloy, and throughout the entire sample, the ferromagnetic–antiferromagnetic transition occurs almost instantaneously, which manifests itself in the sharper curves of the magnetization and electrical resistance vs. temperature.

We summarize in Table 2 the literature data for quenched samples with heat treatment protocols close to those used in this work.

Table 2. Reported quenching protocols and transition parameters after heat treatment, where T_{AFM-FM} and T_{FM-AFM} represent the AFM–FM and FM–AFM transition temperatures and τ the hysteresis width.

Sample	Treatment Protocol	T_{AFM-FM} , K	T_{FM-AFM} , K	τ , K	Type of Measurement	Ref.
Fe ₄₉ Rh ₅₁	Annealing 1273 K, 72 h in vacuum, quenching in air	320.5	314	6.5	M(T) at 0.1 T	[17]
		314	308	6	M(T) at 1 T	
Fe ₄₈ Rh ₅₂	Annealing 1273 K, 336 h in vacuum, quenching in water	321	318	3	M(T) at 1 T	[28]
Fe _{49.5} Rh _{50.5}	Annealing 1370 K, 48 h in vacuum, quenching in water	309	300	9	$\rho(T)$	[29]
Fe ₄₉ Rh ₅₁	Annealing 1273 K, 168 h in vacuum, quenching in air	316	308.5	7.5	M(T) at 1 T	[34]
Fe ₄₉ Rh ₅₁	Annealing 1273 K, 48 h in vacuum, quenching in ice water	329	318	11	M(T) at 5 mT	[40]

We suggest that the origin of the AFM–FM transition plays a significant role in the nuclei of a γ phase arising in the annealing process. This is based on our data, namely from the strong dependence of magnetic transition parameters on annealing temperatures, which may indicate the existence of this phase. These γ phase regions, dispersed in the main magnetic phase, induce a local stress field, affect the magnetic state due to induced deformations, and eventually serve as a nucleus of the FM–AFM transition.

The independence of the transition parameters from the lower quenching temperatures, and the strong dependence on the upper quenching temperatures, shows that this phenomenon can only occur with the alloy structure. To obtain a complete picture of the process, it is necessary to carry out extensive structural studies of alloys at high temperatures. There are more explanations for the heat treatment effect on the magnetic properties of the Fe–Rh alloys in the literature. Chirkova et al. [28] and Takahashi et al. [29] point out the phase decomposition from the α (B2) to α (B2) + γ phases occurring in the alloy with annealing as a reason for the changes in the parameters of magnetic phase transitions. Additional studies are required to elucidate the reasons for the effects of heat treatment on the magnetic and transport properties of Fe–Rh alloys.

4. Conclusions

We have studied the influence of different annealing regimes (changing the upper and lower temperatures of quenching and exposure time) on the first-order AFM–FM transition parameters in Fe₄₉Rh₅₁ alloy. The sharpness of the magnetic transition is increased with the increase of upper quenching temperatures and are almost independent of lower quenching temperatures. As a result, we determined the optimal regime of heat treatment for observation of the transition with parameters close to the “model”: annealing at 1300 K with an exposure time of 440 min and quenching from an upper temperature of 1300 K to a lower temperature of 275 K. The results obtained in this study show how to tune the AFM–FM transition parameters. It is necessary to quench the material within a certain temperature range, during which some changes in the alloy structure or phase decomposition occur.

Author Contributions: Conceptualization, A.A. (Akhmed Aliev), M.A., V.R. (Valeria Rodionova); methodology, M.A., A.A. (Abdulkarim Amirov); validation, A.G.; formal analysis, A.G., E.L.; investigation, M.A., V.R. (Vladimir Rodionov); data curation, M.A., A.A. (Abdulkarim Amirov); writing—original draft preparation, V.R. (Valeria Rodionova), M.A.; writing—review and editing, A.G., V.R. (Valeria Rodionova), A.A. (Abdulkarim Amirov), A.A. (Akhmed Aliev), E.L.; visualization, A.A. (Abdulkarim Amirov); supervision, V.R. (Valeria Rodionova); project administration, V.R. (Valeria Rodionova); funding acquisition, V.R. (Valeria Rodionova). All authors have read and agreed to the published version of the manuscript.

Funding: The work was supported by the Russian Science Foundation, grant No.18-79-10176. E.L. acknowledges support from the Academy of Finland, grant No. 318405 and 333805. The discussion of results has been made possible through the mobility grant provided by the 5 top 100 Russian Academic Excellence Project at Immanuel Kant Baltic Federal University.

Institutional Review Board Statement: Not applicable.

Informed Consent Statement: Not applicable.

Data Availability Statement: The data that support the findings of this study are available from the corresponding author upon reasonable request.

Conflicts of Interest: The authors declare no conflict of interest.

References

- Fullerton, J. The 2017 Magnetism Roadmap. *J. Phys. D Appl. Phys.* **2017**, *50*, 363001.
- Franco, V.; Blázquez, J.S.; Ipus, J.J.; Law, J.Y.; Moreno-Ramírez, L.M. Magnetocaloric effect: From materials research to refrigeration devices. *Conde Prog. Mater. Sci.* **2018**, *93*, 112–232. [\[CrossRef\]](#)
- Liu, J.; Gottschall, T.; Skokov, K.P.; Moore, J.D.; Gutfleisch, O. Giant magnetocaloric effect driven by structural transitions. *Nat. Mater.* **2012**, *11*, 620–626. [\[CrossRef\]](#)
- Annaorazov, M.P.; Asatryan, K.A.; Myalikhgulyev, G.; Nikitin, S.A.; Tishin, A.M.; Tyurin, A.L. Alloys of the FeRh system as a new class of working material for magnetic refrigerators. *Cryogenics* **1992**, *32*, 867–872. [\[CrossRef\]](#)
- Aliev, A.M.; Batdalov, A.B.; Khanov, L.N.; Kamantsev, A.P.; Koledov, V.V.; Mashirov, A.V.; Shavrov, V.G.; Grechishkin, R.M.; Kaul, A.R.; Sampath, V. Reversible magnetocaloric effect in materials with first order phase transitions in cyclic magnetic fields: Fe₄₈Rh₅₂ and Sm_{0.6}Sr_{0.4}MnO₃. *Appl. Phys. Lett.* **2016**, *109*, 202407. [\[CrossRef\]](#)
- Nikitin, S.A.; Myalikhgulyev, G.; Tishin, A.M.; Annaorazov, M.P.; Asatryan, K.A.; Tyurin, A.L. The magnetocaloric effect in Fe₄₉Rh₅₁ compound. *Phys. Lett. A* **1990**, *148*, 363–366. [\[CrossRef\]](#)
- Popescu, A.; Rodriguez-Lopez, P.; Haney, P.M.; Wood, L.M. Thermally driven anomalous Hall effect transitions in FeRh. *Phys. Rev. B* **2018**, *97*, 140407. [\[CrossRef\]](#) [\[PubMed\]](#)
- Arreguín-Hernández, M.L.; Sánchez-Valdés, C.F.; Sánchez Llamazares, J.L.; Ríos-Jara, D.; Pecharsky, V.K.; Blinov, M.I.; Prudnikov, V.N.; Kovalev, B.B.; Zverev, V.I.; Tishin, A.M. Magnetoelastic transition and magnetocaloric effect in induction melted Fe_{100-x}Rh_x bulk alloys with x = 50, 51. *J. Alloy Compd.* **2021**, *871*, 159586. [\[CrossRef\]](#)
- Batdalov, A.B.; Aliev, A.M.; Khanov, L.N.; Kamantsev, A.P.; Mashirov, A.V.; Koledov, V.V.; Shavrov, V.G. Specific heat, electrical resistivity, and magnetocaloric study of phase transition in Fe₄₈Rh₅₂ alloy. *J. Appl. Phys.* **2020**, *128*, 013902. [\[CrossRef\]](#)
- Baranov, N.V.; Barabanova, E.A. Electrical resistivity and magnetic phase transitions in modified FeRh compounds. *J. Alloys Compd.* **1995**, *219*, 139–148. [\[CrossRef\]](#)
- Churyukanova, M.; Kaloshkina, S.; Shuvaeva, E.; Mitra, A.; Pand, A.K.; Roy, R.K.; Murugaiyan, P.; Corte-Leon, P.; Zhukova, V.; Zhukov, A. The effect of heat treatment on magnetic and thermal properties of Finemet-type ribbons and microwires. *J. Magn. Mater.* **2019**, *492*, 165598. [\[CrossRef\]](#)

12. Kamantsev, A.P.; Amirov, A.A.; Koshkid'ko, Y.S.; Mejía, C.S.; Mashirov, A.V.; Aliev, A.M.; Koledov, V.V. Shavrov Magnetocaloric effect in alloy Fe₄₉Rh₅₁ in pulsed magnetic fields up to 50 T. *Phys. Solid State* **2020**, *62*, 161–163. [[CrossRef](#)]
13. Tohki, A.; Aikoh, K.; Iwase, A.; Yoneda, K.; Kosugi, S.; Kume, K.; Batchuluun, T.; Ishigami, R.; Matsui, T.J. Effect of high temperature annealing on ion-irradiation induced magnetization in FeRh thin films. *Appl. Phys.* **2012**, *111*, 07A742. [[CrossRef](#)]
14. Zakharov, A.I.; Kadomtseva, A.M.; Levitin, R.Z.; Ponyatovskii, E.G. Magnetic and magnetoelastic properties of a metamagnetic iron-rhodium alloy. *Soviet Phys. JETP* **1964**, *19*, 1348.
15. Walter, P.H.L. Exchange Inversion in Ternary Modifications of Iron Rhodium. *J. Appl. Phys.* **1964**, *35*, 938–939. [[CrossRef](#)]
16. Polovov, V.M.; Ponomarev, B.K.; Antonov, V.E. Some peculiarities of thermodynamics of transition antiferro-ferromagnetism in iron-rhodium alloys. *Fiz. Met. I Metalloved.* **1975**, *39*, 977–986.
17. Amirov, A.A.; Cugini, F.; Kamantsev, A.P.; Gottschall, T.; Solzi, M.; Aliev, A.M.; Spichkin, Y.I.; Koledov, V.V.; Shavrov, V.G. Direct measurements of the magnetocaloric effect of Fe₄₉Rh₅₁ using the mirage effect. *J. Appl. Phys.* **2020**, *127*, 233905. [[CrossRef](#)]
18. Stern-Taulats, E.; Castan, T.; Planes, A.; Lewis, L.H.; Barua, R.; Pramanick, S.; Majumdar, S.; Manosa, L. Giant multicaloric response of bulk Fe₄₉Rh₅₁. *Phys. Rev. B* **2017**, *95*, 104424. [[CrossRef](#)]
19. Flippen, R.B.; Darnell, F.J. Entropy Changes of Ferromagnetic-Antiferromagnetic Transitions from Magnetic Measurements. *J. Appl. Phys.* **1963**, *34*, 1094–1095. [[CrossRef](#)]
20. Zakharov, A. Crystal lattice parameter and structural distortions in Fe-Rh alloy during phase transformations. *Fiz. Met. I Metalloved.* **1967**, *24*, 84–90.
21. Kouvel, J.S. Unusual Nature of the Abrupt Magnetic Transition in FeRh and Its Pseudobinary Variants. *J. Appl. Phys.* **1966**, *37*, 1257. [[CrossRef](#)]
22. Wayne, R. Pressure Dependence of the Magnetic Transitions in Fe-Rh Alloys. *Phys. Rev.* **1968**, *170*, 523–527. [[CrossRef](#)]
23. Stern-Taulats, E.; Planes, A.; Lloveras, P.; Barrio, M.; Tamarit, J.-L.; Pramanick, S.; Majumdar, S.; Frontera, C.; Manosa, L. Barocaloric and magnetocaloric effects in Fe₄₉Rh₅₁. *Phys. Rev. B* **2014**, *89*, 214105. [[CrossRef](#)]
24. Cherifi, R.O.; Ivanovskaya, V.; Phillips, L.C.; Zobelli, A.; Infante, I.C.; Jacquet, E.; Garcia, V.; Fusil, S.; Briddon, P.R.; Guiblin, N.; et al. Electric-field control of magnetic order above room temperature. *Nat. Mater.* **2014**, *13*, 345. [[CrossRef](#)] [[PubMed](#)]
25. Amirov, A.A.; Baraban, I.A.; Grachev, A.A.; Kamantsev, A.P.; Rodionov, V.V.; Yusupov, D.M.; Rodionova, V.V.; Sadovnikov, A.V. Voltage-induced strain to control the magnetization of bi FeRh/PZT and tri PZT/FeRh/PZT layered magnetoelectric composites. *AIP Adv.* **2020**, *10*, 025124. [[CrossRef](#)]
26. Amirov, A.A.; Rodionov, V.V.; Starkov, I.A.; Starkov, A.S.; Aliev, A.M. Magneto-electric coupling in FeRh -PZT multiferroic composite. *J. Magn. Magn. Mater.* **2019**, *470*, 77–80. [[CrossRef](#)]
27. Lommel, J.M. Effects of Mechanical and Thermal Treatment on the Structure and Magnetic Transitions in FeRh. *J. Appl. Phys.* **1967**, *38*, 1263. [[CrossRef](#)]
28. Chirkova, A.; Bittner, F.; Nenkov, K.; Schultz, N.V.B.L.; Nielsch, K.; Woodcock, T.G. The effect of the microstructure on the antiferromagnetic to ferromagnetic transition in FeRh alloys. *Acta Mater.* **2017**, *131*, 31–38. [[CrossRef](#)]
29. Takahashi, M.; Oshima, R. Annealing Effect on Phase Transition of Equiatomic FeRh Alloy. *Mater. Trans. JIM* **1995**, *36*, 735–742. [[CrossRef](#)]
30. Manekar, M.; Roy, S.B. Very large refrigerant capacity at room temperature with reproducible magnetocaloric effect in Fe_{0.975}Ni_{0.025}Rh. *J. Phys. D Appl. Phys.* **2011**, *44*, 242001. [[CrossRef](#)]
31. Barua, R.; Jimenez-Villacorta, F.; Lewis, L.H. Towards tailoring the magnetocaloric response in FeRh-based ternary compounds. *J. Appl. Phys.* **2014**, *115*, 17A903. [[CrossRef](#)]
32. Kosugi, S.; Fujita, N.; Matsui, T.; Hori, F.; Saitoh, Y.; Ishikawa, N.; Okamoto, Y.; Iwase, A. Modification of magnetic properties of FeRh intermetallic compounds by energetic ion beam bombardment. *Nucl. Instrum. Methods B* **2009**, *267*, 1612–1615. [[CrossRef](#)]
33. Kushwaha, P.; Lakhani, A.; Rawat, R.; Chaddah, P. Influence of thermal annealing and magnetic field on first order magnetic transition in Pd substituted FeRh. *J. Phys. Conf. Ser.* **2010**, *200*, 032038. [[CrossRef](#)]
34. Chirkova, A.; Skokov, K.; Schultz, L.; Baranov, N.; Gutfleisch, O.; Woodcock, T. Magnetic response of FeRh to static and dynamic disorder. *Acta Mater.* **2016**, *106*, 15–21. [[CrossRef](#)]
35. Chichay, K.; Rodionova, V.; Zhukova, V.; Kaloshkin, S.; Churyuknova, M.; Zhukov, A.J. Investigation of the magnetostriction coefficient of amorphous ferromagnetic glass coated microwires. *Appl. Phys.* **2014**, *116*, 173904. [[CrossRef](#)]
36. Swartzendruber, L.J. The Fe–Rh (Iron-Rhodium) system. *Bull. Alloy Phase Diagr.* **1984**, *5*, 456–462. [[CrossRef](#)]
37. Okamoto, H.J. Phase Equilibria Diffus. *J. Phase Equilibria Diffus.* **2011**, *32*, 472. [[CrossRef](#)]
38. Pal, L.; Tarnocz, T.; Szabo, P.; Kren, E.; Toth, J. Investigation of antiferromagnetic-ferromagnetic transformation in iron-rhodium alloys. *Proc. Int. Conf. Magn. (Nottingham)* **1964**, 158–161.
39. Zverev, V.I.; Saletsky, A.M.; Gimaev, R.R.; Tishin, A.M.; Miyanaga, T.; Staunton, J.B. Influence of structural defects on the magnetocaloric effect in the vicinity of the first order magnetic transition in Fe_{50.4}Rh_{49.6}. *Appl. Phys. Lett.* **2016**, *108*, 192405. [[CrossRef](#)]
40. Sánchez-Valdés, C.F.; Gimaev, R.R.; López-Cruz, M.; Llamazares, J.L.S.; Zverev, V.I.; Tishin, A.M.; Carvalho, A.M.G.; Aguiar, D.J.M.; Mudryk, Y.; Pecharsky, V.K. The effect of cooling rate on magnetothermal properties of Fe₄₉Rh₅₁. *J. Magn. Magn. Mater.* **2020**, *498*, 166130. [[CrossRef](#)]